

Microwave and Acoustic Absorption Metamaterials

Sichao Qu[✉]* and Ping Sheng[✉][†]

Department of Physics, The Hong Kong University of Science and Technology, Clear Water Bay, Kowloon, Hong Kong, China



(Received 27 February 2022; revised 28 March 2022; accepted 5 April 2022; published 27 April 2022)

Wave-absorption metamaterials have been an enduring topic over the past two decades, propelled not only by scientific advances, but also by their extensive application potential. In this review, we aim to provide some general insights into the absorption mechanism common to both microwave and acoustic systems. By establishing a universal model for resonance-based metamaterials, we present the theoretical conditions for broadband impedance matching and introduce the fundamental causal limit as an evaluation tool for absorption performance. Under this integrated framework, we survey recent advances in metamaterial absorption in both microwave and acoustic systems, with a focus on those that have pushed the overall performance close to the causal limit. We take note of some emerging metastructures that can circumvent the constraints imposed by causal limit, thereby opening an avenue to low-frequency absorption. This review concludes by discussing the existing challenges with possible solutions and the broad horizon for future developments.

DOI: 10.1103/PhysRevApplied.17.047001

I. INTRODUCTION

Wave absorption is important to many aspects of our daily life. We rely on ultraviolet absorption by atmospheric molecules to protect us from skin damage. Solar cells absorb sunlight through the photovoltaic mechanism to provide green energy. The capture and processing of ubiquitous microwave signals are now the basis of high-speed communication that is indispensable in our society. We install sound-absorbing materials in buildings to alleviate noise problems and/or improve the indoor auditory experience. In view of such diverse significance of wave absorption, the development of high-performance broadband absorbers has long been a widely pursued topic. However, for traditional materials [1,2], such as porous absorptive foam, there are inherent restrictions on material properties, thereby leading to the low tunability of the absorption spectrum. Thanks to the development of metamaterials [3–9], which are artificial composite structures that rely on the interaction between the structural geometry, material characteristics, and wave properties for the resulting wave-manipulation capabilities, we are now presented with myriad possibilities to tune metamaterial functionalities that cannot be found in nature. In particular, it becomes possible to customize the absorption spectrum according to specific targets in different application scenarios.

An essential element in absorber design is impedance matching in the desired frequency band to avoid reflection from the sample. However, it turns out that associated with impedance matching there is another important consideration: sample thickness. In practice, it is always a challenge to attain high dissipation in the low-frequency range within a given wavelength, because, for any linear response system, the dissipation coefficient is a quadratic function of frequency [10]. Even if some metamaterials can take advantage of the low-frequency modes to achieve excellent absorption with a thin sample thickness, we see that their operating bandwidth is usually extremely narrow. Therefore, a natural question arises: is there some general constraint between the absorption spectrum and the sample thickness? The answer turns out to be “yes” for arbitrary linear, passive, and time-invariant systems. Theoretical studies reveal that the integral of the reflection coefficient on the logarithmic decibel (dB) scale, concerning wavelength, represents a minimum sample thickness (apart from some constants) that must be smaller than the actual sample thickness. This well-known relationship is called the *causal limit* or *causality constraint* [11,12]. Therefore, for a given available space, we can know in advance the maximal absorption performance over the desired frequency band [13]. One can also turn the causal limit into an effective evaluation tool [14] for optimizing absorber performance to approach the *causal optimality* through iterations of the absorber design parameters.

The integrated consideration of impedance matching and causal limit provides an objective perspective for

*squ@connect.ust.hk

[†]sheng@ust.hk

this review article to survey the microwave and acoustic absorption metamaterials. In what follows, we first make concrete the theoretical framework in Sec. II by superposing Lorentzian functions, which can be used to analyze any linear wave systems with the causal response. Based on this framework, we derive the theoretical conditions for an absorber to achieve broadband impedance-matching conditions while simultaneously also approaching the causal limit. This is followed by a survey of the representative works in the microwave and airborne acoustic absorption systems in Sec. III. In particular, we focus on the transition from local resonances to broadband absorption along the development trajectory of metamaterial absorbers. Defined by the causal limit, optimal broadband absorbers are observed to emerge with diverse design approaches. Section IV notes very recent works that can mitigate or circumvent the restriction imposed by the original causal limit. We conclude in Sec. V by delineating the challenges faced by metamaterial absorbers in the transition to products and the broad horizons when such challenges can be met.

II. A THEORETICAL MODEL FOR RESONANCE-BASED METAMATERIALS

A. Model definitions

Due to the subwavelength feature of metamaterials, we model the wave-absorption phenomenon as a one-dimensional problem (i.e., normal incidence) for simplicity. This is justified because, even at oblique incidence, the phase difference across the subwavelength sample surface is small, as long as the incidence angle is not close to 90° . To unify the description of both microwave and acoustic systems, we adopt the following mapping [15]: $\phi \rightarrow H$, p for magnetic field and acoustic pressure modulation, respectively; while the counterpart to ϕ is φ , which denotes either the electric field, E , or acoustic (particle) displacement velocity, v . It is understood that the electromagnetic (EM) fields are transverse (TEM mode), and the acoustic field, p , is scalar in character, with a longitudinal velocity field, v . We note that both ϕ_i and ϕ_r , where the subscripts i , r denote incidence and reflection, respectively, are plane waves with the phase variation $e^{i(kx-\omega t)}$, where k , ω denote the wavevector and angular frequency, respectively, while x represents the direction of wave propagation and t is time.

In Fig. 1(a), consider an incident field ϕ_i incident on the interface between the air and metamaterials, defined to be at $x = 0$. Imperfect impedance matching would cause a backward reflected field, ϕ_r . To eliminate transmission, we specify a Neumann boundary condition, $\partial_x \phi|_{x=d} = 0$, on the backside of the sample (i.e., perfect electric conductor boundary for the EM case and a hard boundary for the acoustic case). The reflection coefficient is given by

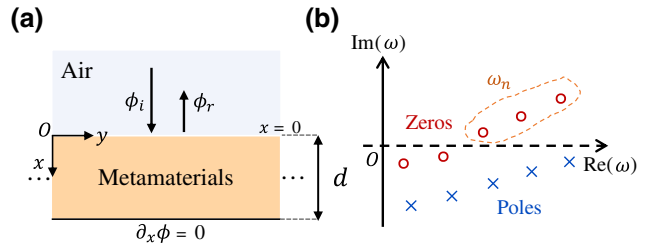


FIG. 1. (a) Schematic illustration of the metamaterial absorbing layer, modeled as a one-dimensional problem. ϕ_i is the incident field and ϕ_r is the reflected field. Total field, $\phi = \phi_i + \phi_r$. (b) Complex frequency plane of $\ln(|R|)$ with a schematic illustration for the locations of its zeros (red circles) and poles (blue crosses). Dots encircled by the dashed line are the set of ω_n defined on the upper complex plane, where $\text{Im}(\omega_n) > 0$.

$$R = \left. \frac{\phi_r}{\phi_i} \right|_{x=0} = \frac{Z_s - Z_c}{Z_s + Z_c}, \quad (1)$$

where Z_c denotes the generalized impedance of the incident medium, i.e., the characteristic admittance, $\sqrt{\epsilon_0/\mu_0}$, in the EM case or characteristic impedance, $\sqrt{\rho_0 B_0}$, in the acoustic case. Here, ϵ_0 and μ_0 denote permittivity and permeability, respectively, in the EM case, while ρ_0 and B_0 denote mass density and bulk modulus, respectively, in the acoustic case. The generalized surface impedance, Z_s , is defined by

$$Z_s = \left. \frac{\phi}{\varphi} \right|_{x=0}, \quad (2)$$

where both ϕ and φ are the total fields (summation of the forward and backward waves). In the absence of transmission, the absorption coefficient is given by $A = 1 - |R|^2$, according to energy conservation, which can be further expressed as

$$A = 1 - \left| \frac{Z_s - Z_c}{Z_s + Z_c} \right|^2. \quad (3)$$

Impedance matching is realized when $Z_s = Z_c$, at which $A = 1$. For the ease of ensuing theory formulation, we introduce the Green function, $G(x, x')$ [15,16], to characterize the response of metamaterials. In particular, by investigating the surface response ($x = x' = 0$), we can link Z_s with $G(\omega)$ by

$$G(\omega) = \frac{1}{-i\omega Z_s}. \quad (4)$$

From Eq. (4), we learn that the surface impedance, Z_s , can be obtained once $G(\omega)$ is known.

B. Green function for multiple resonances

Within a metamaterial, multiple resonant states can be excited by an incident wave. By projecting these states onto the material-air interface, we can obtain the overall response, given by the superposition of the Lorentzian functions

$$G(\omega) = \sum_{i=1}^N \frac{\alpha_i}{\omega_i^2 - \omega^2 - i\beta_i\omega}, \quad (5)$$

where ω_i , α_i , and β_i are the i th resonance frequency, oscillation strength, and dissipation factor, respectively. The coefficients (ω_i , α_i , and β_i) in $G(\omega)$ can be expressed in terms of the eigenfunctions of the absorption sample, which may be evaluated either analytically, when possible, or numerically, when analytical solutions are difficult to obtain. The eigenfunctions are defined as those obtained by setting the Dirichlet boundary condition on the sample surface, which is, thus, nonradiating in nature. For related examples of mode-expansion theory, one can refer to Ref. [17] and Ref. [15] for EM and acoustic metamaterials, respectively.

We note that, since each Lorentzian function follows the Kramers-Kronig relations [18], which is derived based on the assumption of linearity and causality, the summation $G(\omega)$ must also inherit these properties. In fact, Dirdal and Skaar [19] rigorously proved that all causal functions could be approximated by the superpositions of Lorentzian functions to arbitrary precision. Therefore, starting from Eq. (5), our model is universal and can be used to describe any causal wave system, which serves as one of the theoretical bases of our following analysis of the resonance-based metamaterials.

C. Causal limit as an evaluation tool

For any linear and passive absorber, its reflected wave, $\phi_r(t)$, can depend only on the incident wave before the current time instant, t . Mathematically, it can be formulated in the form of a convolution integral:

$$\phi_r(t) = \int_0^\infty K(\tau)\phi_i(t-\tau)d\tau, \quad (6)$$

where $K(\tau)$ is the response kernel function in the time domain, the Fourier transform of which gives the reflection coefficient in the frequency domain, i.e., $R(\omega) = \mathcal{F}\{K(\tau)\}$. By analyzing the analyticity of a derivative function containing $R(\omega)$, we can obtain the following relationship [11,12,20]:

$$-\int_0^\infty \ln|R(\omega)| \frac{d\omega}{\pi\omega^2} = \frac{d}{c_0 F} - \sum_n \frac{\text{Im}(\omega_n)}{|\omega_n|^2}. \quad (7)$$

Here, d is the thickness of the absorber, c_0 is the wave speed in the ambient environment, and ω_n denotes the

zeros of $\ln(|R|)$ that are located in the upper half-plane of the complex frequency plane, i.e., $\text{Im}(\omega_n) > 0$ [see Fig. 1(b)]. For the EM and acoustic cases, the dimensionless factor, F is defined by

$$F = \begin{cases} \lim_{\omega \rightarrow 0} \frac{B_{\text{eff}}(\omega)}{B_0} & (\text{acoustic}), \\ \lim_{\omega \rightarrow 0} \frac{\mu_{\text{eff}}(\omega)}{\mu_0} & (\text{EM}), \end{cases} \quad (8)$$

with μ_{eff} and B_{eff} being the effective permeability and effective bulk modulus, respectively, of the metamaterials at the static limit $\omega \rightarrow 0$. Since the summation term in Eq. (7) is always positive, we can alternatively turn Eq. (7) into an inequality, known as the *causal limit*:

$$d \geq d_{\min} = \frac{F}{4\pi^2} \left| \int_0^\infty \ln|1 - A(\lambda)| d\lambda \right|, \quad (9)$$

where we substitute reflection R with absorption A and angular frequency ω with wavelength, λ . d_{\min} is noted to be the minimal thickness dictated by the causal limit. We learn from Eq. (9) that perfect absorption for all frequencies is impossible with a finite sample thickness, i.e., the integral does not converge. Also, to some extent, Eq. (9) explains why the low-frequency absorption is difficult with a thin sample because the long-wavelength part of the integral is dominant in determining the value of d_{\min} .

We introduce a causality ratio [14] as a tool for evaluating the absorption performance; this is given by

$$R_c = \frac{d}{d_{\min}}. \quad (10)$$

If $R_c = 1$, all the zeros [red circles in Fig. 1(b)] must shift to the lower plane, and thus, the absorber is defined as causally “optimal” [14,20]. We show this condition to be achievable by increasing either the dissipation or the mode density. It should be noted that, if there is a zero exactly on the real frequency axis in Fig. 1(b), such a condition is regarded as *critical coupling* [21], which, however, is not the necessary condition for causal optimality.

We emphasize that, when evaluating the performance of an absorber, the evaluation index, R_c , should be used together with the operating bandwidth, since a single-band absorber can also realize $R_c = 1$ (see examples in Ref. [13]). Therefore, in what follows, we derive the condition for broadband impedance matching while exploring how to approach the causal optimality simultaneously.

D. Theoretical conditions for broadband impedance matching

Consider an idealized collection of resonances with a continuum distribution of resonance frequencies, i.e., $\Omega \in [\omega_1, \infty)$. We define the mode density as $D(\omega) = dN/d\omega$,

where dN is the mode number within the frequency interval $[\omega, \omega + d\omega]$. Then, Eq. (5) can be alternatively formulated as

$$G(\omega) = \int_{\omega_1}^{\infty} \frac{\alpha(\Omega)D(\Omega)}{\Omega^2 - \omega^2 - i\omega\beta(\Omega)} d\Omega, \quad (11)$$

which can be divided into real and imaginary parts as follows. Based on the small dissipation assumption (i.e., $\beta \ll \omega$), we can utilize the asymptotic definition of the Dirac delta function [22] to obtain

$$\begin{aligned} G(\omega) &= P \int_{\omega_1}^{\infty} \frac{\alpha(\Omega)D(\Omega)}{\Omega^2 - \omega^2} d\Omega \\ &\quad + i\pi \int_{\omega_1}^{\infty} \alpha(\Omega)D(\Omega)\delta(\Omega^2 - \omega^2)d\Omega. \end{aligned} \quad (12)$$

The principal value of the first term on the right-hand side can be approximately treated as zero for $\omega > \omega_1$. Our present target is to attain impedance matching over a broadband frequency range above ω_1 . According to Eq. (3), this requires $\text{Im}[G(\omega)] \cong 1/(\omega Z_c)$. Therefore, by combining this target with Eq. (12), we have the *impedance-matching condition* for the continuum model:

$$\alpha(\omega)D(\omega) = \frac{2}{\pi Z_c}. \quad (13)$$

By substituting Eq. (13) back into Eq. (11), an analytical form for idealized continuous resonances can be derived

from

$$G(\omega) = \lim_{\beta \rightarrow 0} \int_{\omega_1}^{\infty} \frac{2/(\pi Z_c)}{\Omega^2 - \omega^2 - i\beta\omega} d\Omega, \quad (14)$$

which can be further reduced to

$$G(\omega) = \begin{cases} \frac{1}{\omega\pi Z_c} \ln\left(\frac{\omega_1 + \omega}{\omega_1 - \omega}\right), & \text{if } \omega < \omega_1, \\ \frac{1}{\omega Z_c} \left[i + \frac{2}{\pi} \tanh^{-1}\left(\frac{\omega_1}{\omega}\right) \right], & \text{if } \omega > \omega_1, \end{cases} \quad (15)$$

which is plotted as dashed lines in the upper panels of Fig. 2. In Eq. (15), the disappearance of $\text{Im}(G)$ below ω_1 is due to the assumed nonexistence of mode density below ω_1 ; thus, the absorption must also be zero.

In practice, we can only have a finite number of discretized resonances to approach the causal target given by Eq. (15). Hence, in this case, we define the mode density as $D(\omega_i) = 1/(\omega_{i+1} - \omega_i) = 1/\delta\omega_i$ and the *impedance-matching condition* in Eq. (13) can be modified to fit the discretized model, which is written as

$$\alpha_i = \frac{2\delta\omega_i}{\pi Z_c}. \quad (16)$$

From Eqs. (13) and (16), we learn that the product of the oscillation strength and mode density should be a constant to best attain broadband impedance matching. While this condition is derived for the target of broadband impedance

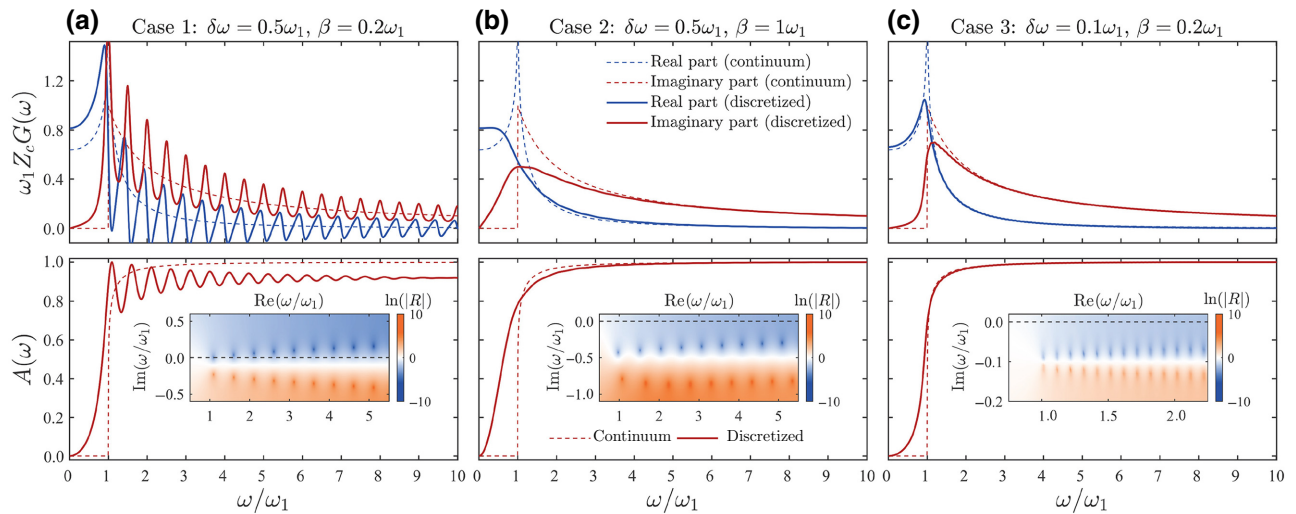


FIG. 2. Green function [in dimensionless form given by $\omega_1 Z_c G(\omega)$] and the corresponding absorption spectrum $A(\omega)$. Dashed lines denote results from the continuum resonance model, given by Eq. (15), which serves as the causal target. Solid lines correspond to the discretized resonance model, given by Eq. (5). Insets are the value of $\ln(|R|)$ on the complex frequency plane. Blue and orange dots are zeros and poles, respectively. (a) Case 1, reference case with relatively low mode density and low dissipation factor ($\delta\omega = 0.5\omega_1$, $\beta = 0.2\omega_1$); (b) case 2, low mode density and high dissipation factor ($\delta\omega = 0.5\omega_1$, $\beta = \omega_1$); (c) case 3, high mode density and low dissipation factor ($\delta\omega = 0.1\omega_1$, $\beta = 0.2\omega_1$).

matching above a cutoff frequency of ω_1 , the present approach can be extended to construct the conditions for attaining arbitrary broadband impedance [23,24].

In what follows, we demonstrate, by using the model of broadband total absorption above a cutoff frequency, how the two parameters—resonance mode density and dissipation coefficient—can be utilized to *approach* the $R_c = 1$ condition. Subsequently, we show, through a survey of metamaterials in the literature, how the development of metamaterial absorbers—from narrow frequency to broadband—has roughly followed the above framework.

E. Relationship between thickness and the static Green function

To consider the model of discretized resonances, we first show, as a reference, the consistency of the continuum model used in previous sections. To this end, we build up the relationship between the absorber's thickness, d , and the static Green function, for the purpose of calculating R_c . We assume a Neumann boundary condition, $\partial_x \phi|_{x=d} = 0$, on the backside of the sample. Therefore, according to the impedance-transfer formula, the surface impedance of the absorber is

$$Z_s = iZ_{\text{eff}}(\omega) \cot[\omega d/c_{\text{eff}}(\omega)], \quad (17)$$

where $Z_{\text{eff}}(\omega)$ and $c_{\text{eff}}(\omega)$ denote the generalized effective impedance and effective wave speed of the metamaterials, respectively. By inserting Eq. (17) into Eq. (4), we have

$$G(\omega) = \frac{\tan[\omega d/c_{\text{eff}}(\omega)]}{\omega Z_{\text{eff}}(\omega)}, \quad (18)$$

the static limit of which allows us to extract the thickness:

$$d = \lim_{\omega \rightarrow 0} c_{\text{eff}}(\omega) Z_{\text{eff}}(\omega) G(\omega), \quad (19)$$

where, at the static limit, $c_{\text{eff}}Z_{\text{eff}} = B_{\text{eff}}$ in the acoustic case and $c_{\text{eff}}Z_{\text{eff}} = 1/\mu_{\text{eff}}$ in the EM case. Based on Eq. (19), we compare d with d_{\min} , and thereby, R_c can be obtained.

F. Evaluation of R_c for continuum and discretized cases

We show analytically that, for the idealized continuum case with the causal impedance form [see Eq. (15)], causal optimality always holds, i.e., $R_c = 1$. However, for the discretized case, which is always the practical case, we numerically demonstrate that the condition $R_c = 1$ is conditional, depending on the locations of the zeros of $\ln(|R|)$ on the complex frequency plane.

1. Idealized continuum case

We revisit the idealized continuum model. By combining Eqs. (19) and (15), we can analytically get the

corresponding thickness:

$$d = \lim_{\omega \rightarrow 0} c_{\text{eff}} Z_{\text{eff}} \frac{1}{\omega \pi Z_c} \ln \left(\frac{\omega_1 + \omega}{\omega_1 - \omega} \right) = \frac{2c_{\text{eff}} Z_{\text{eff}}}{\pi \omega_1 Z_c} = \frac{2Fc_0}{\pi \omega_1}. \quad (20)$$

The minimal thickness dictated by the causal limit can be obtained by inserting Eq. (15) into Eq. (3) and analytically performing the integral in Eq. (9):

$$d_{\min} = \frac{Fc_0}{2\pi} \int_{\omega_1}^{\infty} \ln \left| \frac{i \tanh^{-1}(\omega_1/\omega)}{\pi - i \tanh^{-1}(\omega_1/\omega)} \right| \frac{d\omega}{\omega^2} = \frac{2Fc_0}{\pi \omega_1}, \quad (21)$$

which is exactly the same as that given by Eq. (20). Therefore, the continuum model, based on the impedance-matching condition [Eq. (13)], is self-consistent and causally optimal. This can serve as a target, with its corresponding absorption plotted as dashed lines in the lower panels of Fig. 2, that can be approached by the discretized model (solid lines in Fig. 2).

2. Discretized case

We show that causality optimality does not necessarily hold in the discretized case. By inserting Eq. (5) into Eq. (19), we obtain the thickness given by

$$d = \begin{cases} B_{\text{eff}} \sum_{i=1}^N \alpha_i / \omega_i^2 & (\text{acoustic}), \\ (1/\mu_{\text{eff}}) \sum_{i=1}^N \alpha_i / \omega_i^2 & (\text{EM}). \end{cases} \quad (22)$$

Based on Eq. (22), we compare d with d_{\min} , and thereby R_c can be numerically obtained.

For simplicity of demonstration, we assume all the Lorentzian terms in Eq. (5) have the same dissipation factor ($\beta_i = \beta$) and the resonances are distributed evenly, which means the mode density is constant and is given by

$$D(\omega) = \frac{1}{\omega_{i+1} - \omega_i} = \frac{1}{\delta\omega}. \quad (23)$$

Now, we can demonstrate this with numerical results since analytical forms are not available. We select three cases with different $(\delta\omega, \beta)$ values (displayed in the top panels of Fig. 2), and the oscillation strengths are set accordingly to satisfy the impedance-matching condition given by Eq. (16).

For case 1 (the first column), the mode density is relatively low and the dissipation is also small. As a consequence, the Green function deviates from the target with an oscillating manner, and the absorption also fluctuates around 0.9. In the inset, it is seen that the zeros of $\ln(|R|)$ are on the upper-frequency plane, indicating the system

is not causally optimal. To improve the absorption and to approach the causal limit, we propose two feasible routes. The first one is to increase the dissipation, β , from $0.2\omega_1$ to ω_1 (denoted as case 2). From the results displayed in Fig. 2(b), we can see that the Green function is now closer to the target idealized model. Also, the absorption becomes smooth and flat at a high level. The second route is to increase the mode density by changing $\delta\omega$, from $0.5\omega_1$ to $0.1\omega_1$ (case 3). In this way, the Green function and absorption almost coincide with the targets. We can conclude that both routes are feasible for approaching the idealized continuum model, and thereby, causally optimality [see the insets in Figs. 2(b) and 2(c)]. In Fig. 3, we scan the R_c values by varying $(\beta, \delta\omega)$ and mark the two routes that we demonstrate. The blue color indicates the region with a low R_c close to unity.

The above discussion shows theoretically that if an absorber, with a given sample thickness and absorption spectrum, deviates from the $R_c = 1$ condition, then there is potential for improving the absorption without increasing the sample thickness. Usually that is difficult for traditional absorbers, since it may involve changing the material properties. However, this is precisely the area where metamaterials can help, by tuning the mode density of the resonances and the dissipation coefficient associated with each resonance.

In summary, the theoretical model gives us several important lessons. First, the impedance-matching condition should be satisfied [as Eq. (16)]. In other words, if we regard the modes as harmonic oscillators, the oscillation strength of each one needs to be fitted with the mode density to create a wide absorption-frequency range. The second is that dissipation of the system should also be adapted to the mode density [see the two examples shown

in Figs. 2(b) and 2(c)]. Although an excessive dissipation (β higher than the optimal value) does not negatively affect the causality optimality, it will enhance the absorption below the cutoff ω_1 . In other words, more thickness or space resource would be wasted in the low-frequency part, which would inevitably reduce the overall absorption beyond ω_1 , i.e., the designed operating bands, in accordance with the causal limit. It should also be noted that, even though a higher β may seem to lower the absorption for a particular resonance, when viewed in the context of *broadband* absorption, it is not always a negative feature, because a higher β would spread the absorption of a single resonance to the neighboring frequencies, thereby benefiting the overall absorption. Although our model is relatively simplified compared to the practical cases, the results are of universal significance for the design of broadband absorbers.

III. ABSORPTION BY RESONANCE-BASED METAMATERIALS

Early metamaterial absorbers rely on a single or a few resonant modes to concentrate energy density, thus attaining excellent but usually narrowband absorption with deep subwavelength thicknesses, which is not typically feasible from traditional materials. Meanwhile, the tunability of the absorption frequency is also a feature that has attracted strong interest due to its application value [25]. However, with advances in the understanding of absorption mechanisms, some structures are designed to break the narrowband nature and extend the absorption ability to a wider frequency range. A transition from narrowband to broader-frequency-range absorption is an inevitable step in the evolution of metamaterial absorbers.

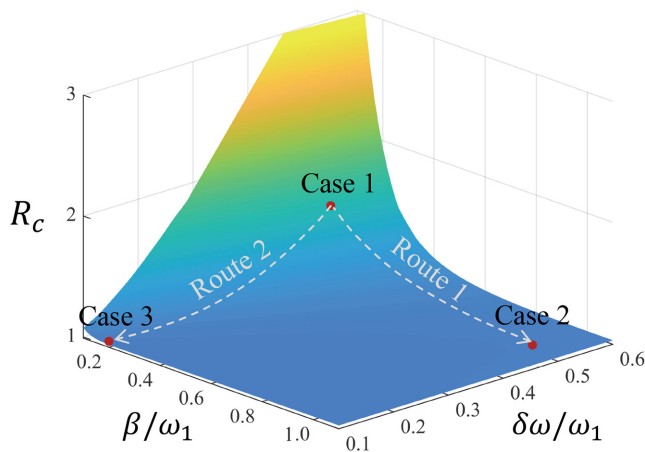


FIG. 3. Value of causality ratio, plotted as a function of dimensionless parameters β and $\delta\omega$. Variation of $(\beta, \delta\omega)$ represents two options to achieve causal optimality.

A. Microwave absorbers

Microwave is the most-challenging frequency regime for absorption among diverse EM bands, due to its long wavelength and high penetrability through solids. Driven by the need for applications related to radar, Dallenbach [26] and Salisbury [27] absorbers were the earliest examples, to the best of our knowledge. These early microwave absorbers share similar absorption mechanisms based on quarter-wavelength resonances fitted with a lossy layer. However, such classical absorbers [28–30] are usually thick in low-frequency absorption because of their requirements for quarter wavelength. More recently, an early metamaterial-based absorber was proposed by Landy *et al.* [31], with a thickness only 1/35 of the relevant wavelength [see Fig. 4(a)]. The split-ring structure is responsible for enhancing the electric couplings, while the cut line behind can support a magnetic response. In this way, effective permittivity and permeability can be decoupled and their

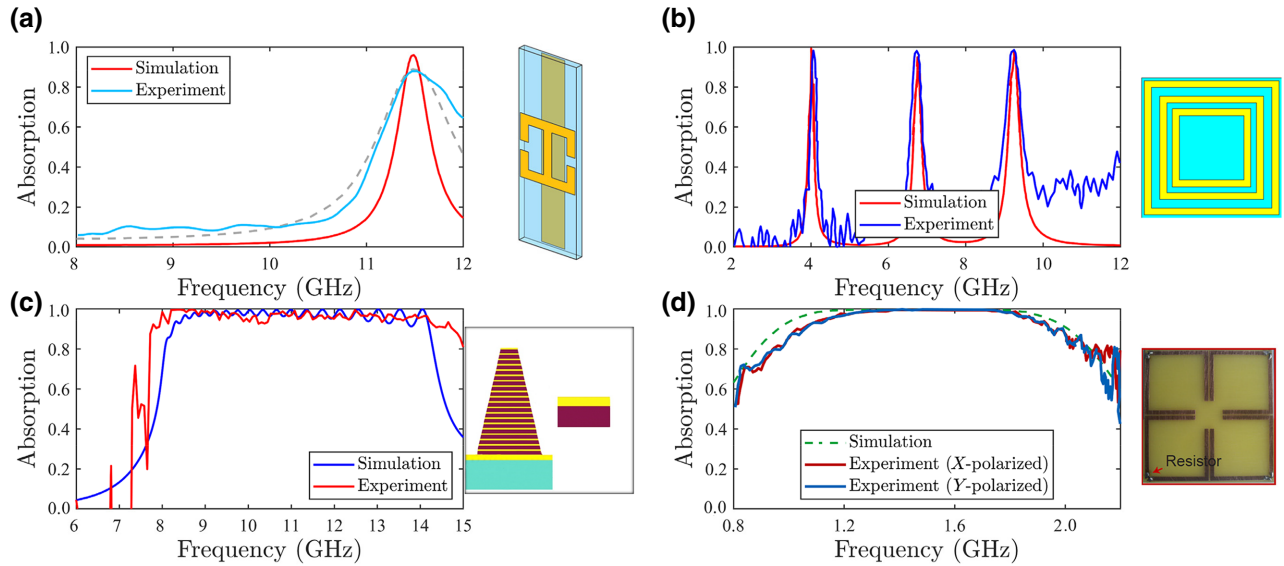


FIG. 4. Performance and structure of microwave metamaterial absorbers. (a) Single-band absorber with high absorption at 11.5 GHz. (b) Triple-band absorber with concentric three-metal-ring structure. (c) Multilayer absorber with a wide absorption band, facilitated by stacked patch resonators. (d) Low-frequency wideband absorber equipped with four resistive metallic rings. For (a),(b), sample schematics are plotted from the top view, i.e., incident wavevector is perpendicular to the plane of the structure. For (c),(d), samples are viewed from the side, with incident wavevector in the plane of the illustration. Reused with permission from Refs. [31–34].

respective resonances can be individually tuned. However, such narrowband absorption at a single frequency [31,35–38] may have only limited applications.

To extend the absorption-frequency bands, one can either increase the resonance mode density (denoted route 1) or the loss of the system (denoted route 2), as previously discussed. Shen *et al.* [32] proposed concentric ring structures to create a triple-band absorber [see Fig. 4(b)]. Many similar works followed, with the aim of achieving perfect absorption by using multiple subwavelength-resonant structures at discrete resonance frequencies [39–41]. Going a step further, Ding *et al.* [33] stacked a 20-layer metal structure to achieve a larger mode density, thus fusing the discrete frequency bands into a continuous band [Fig. 4(c)]. Xiong *et al.* [42] also adopted multilayer metallic strips but used fewer layers to achieve similar broadband effects. The absorbers mentioned above are usually made of metallic structures, embedded in dielectric substrates. Some other materials were also explored to construct diverse microwave absorbers, such as liquid droplets [43–45], indium tin oxide film [46,47], and graphene composites [48,49]. Regardless of the specific composition of the materials, the ultimate goal is to support the resonant modes and to adjust the dissipation.

Sparse metallic structures generally have relatively strong resonant responses and are easy to fabricate with printed-circuit-board (PCB) technologies. However, owing to both the low resistance of the metals and the low ohmic loss of the substrate dielectrics, narrowband-absorption features are difficult to avoid. This problem can be solved

by introducing chip resistors to connect the metallic components. In principle, the resistance of the resistors can be designed to be any value, with infinity corresponding to the open circuit and infinitely small corresponding to the short circuit. Therefore, dissipation in microwave systems is easy to regulate. By using chip resistors, a large body of work [50–52] achieved considerable success in broadband absorption, without many resonators, as shown in Ref. [33]. Ye *et al.* designed a single-band perfectly matched layer [53], and by adding resistively resonant units and optimizing their couplings, the same group extended the perfectly matched layer effect to wider and lower bands (from 1.1 to 2 GHz) [34] [see Fig. 4(d)].

Recently, a design recipe for an ultrabroadband microwave absorber was proposed by Qu *et al.* [14]. They discovered two magnetic resonances with high surface impedance [Fig. 5(a)] could be supported by an electrical dipole resonator in the form of a single metallic ring [Fig. 5(d)], placed close to a perfect electric conductor (PEC) boundary. By fine-tuning the resistance loaded on the ring, the first-order and second-order magnetic resonances inevitably interact with each other [Fig. 5(b)], thereby leading to their coalescence into a broad impedance-matching band [Fig. 5(c)] (using the loaded resistors to manipulate the resonance dispersions is one manipulation approach of *dispersion engineering* [54]). Not surprisingly, the impedance-matching condition leads to a –20-dB reflection loss between 3.6 and 9 GHz [Fig. 5(e)]. Furthermore, as the absorption-frequency band

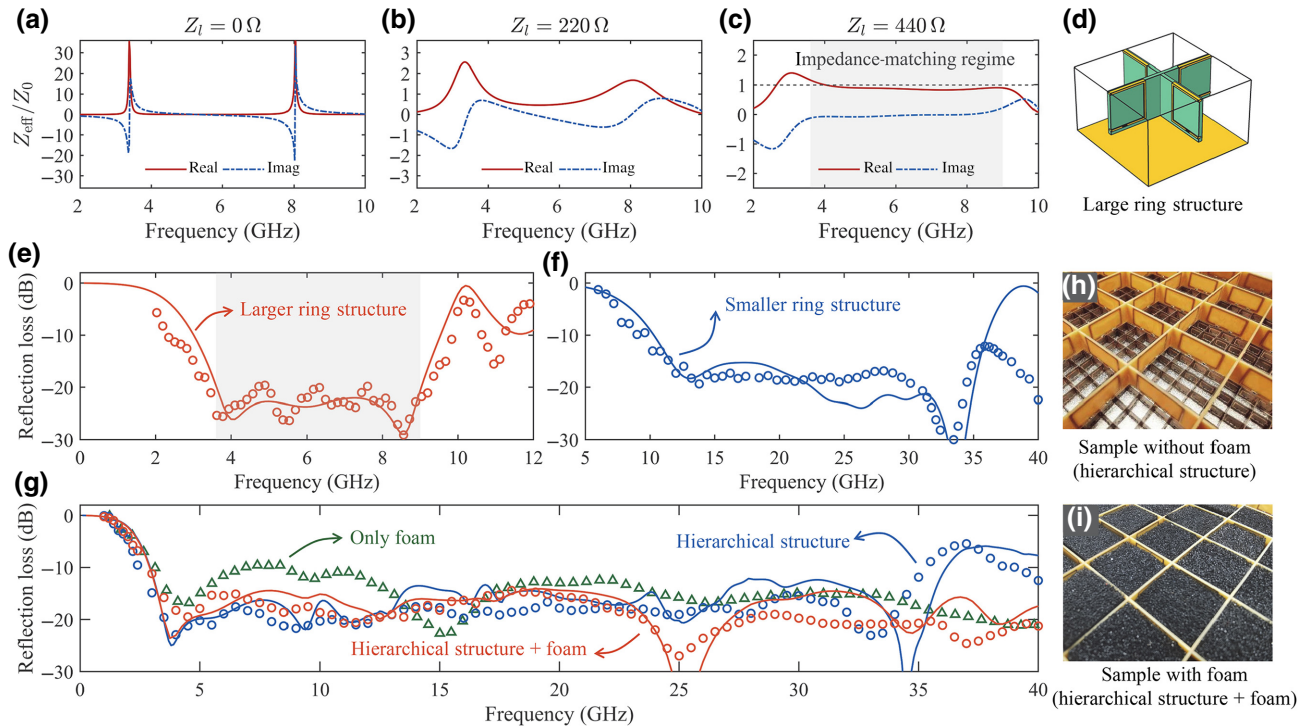


FIG. 5. (a)–(c) Results of dispersion engineering, by tuning the loaded resistance to 0Ω , 220Ω , and 440Ω , respectively. (d) Unit cell of the large ring structure. (e) Absorption performance with the optimal resistance of 440Ω , achieved by a single large ring structure. Solid lines are simulation results while circles are experimental results. Gray shading indicates the impedance-matching frequency regime. (f) Same for the small ring structure. (g) Absorption of foam absorber (green), integrated hierarchical structure (blue), and hierarchical structure with foam (orange). (h),(i) Images of fabricated samples. Reused with permission from Ref. [14].

is always inversely proportional to the relevant size of the absorber, if the size of the unit cell is scaled to $1/4$ (keeping the optimal resistance unchanged), the absorption band of the smaller ring structure will be around 4 times higher [see Fig. 5(f)]. Now, an opportunity to extend the absorption bands arises: the large and small ring structures can be integrated along the wave's incident direction to form a hierarchical structure [Fig. 5(h)], with its absorption spectra spliced as well [blue line and dots in Fig. 5(g)]. However, in such a case, the diffraction inevitably appears due to ultrabroadband coverage. To mitigate this problem, a conventional foam absorber is adopted to efficiently dissipate the additional diffraction beams [see the final combined structure in Fig. 5(i)], and the reflection loss is plotted as the orange line and dots in Fig. 5(g). Therefore, the final operating band (with a minimum of 90% absorption) is from 3 GHz to at least 40 GHz with a causality ratio of $R_c = 1.05$ [14], which means that the causality optimality is achieved in this work. It is worth noting that the traditional material—sponge foam—also has quite a good performance [green triangles in Fig. 5(g)]. This fact reveals that it is not easy for metamaterials to outperform sponge foams in practical applications, but the metamaterial absorbers possess the capability of frequency-band tunability that is absent in traditional materials, which can

be utilized to approach causal optimality in specified target frequency bands.

In addition to moving toward a wider band performance, microwave-absorption metamaterials may also need to be lightweight [55], repairable [56], switchable [57], or optically transparent [46,58] for practical applications. Also, how to achieve better oblique-incidence performance is a problem worthy of further study. The concepts and principles used in the microwave absorber can also be extended to higher bands, such as terahertz [35,36,39, 59–61], infrared [36,37,62,63], and visible light [64–68].

B. Acoustic absorbers

Tuning the dissipation of acoustic systems is not as flexible as that of microwave systems, since the viscosity coefficients of air and solid materials are relatively fixed. Therefore, the main method for broadband absorption in acoustic metamaterials is to increase the resonance mode density (route 2 in Fig. 3). However, in the case of acoustic waves, we can always use hard boundaries to decouple different resonant modes; this is usually difficult in microwave absorbers with resonant elements owing to non-negligible near-field couplings [17], and we do not have the perfect magnetic boundary conductor (PMC) to

confine the electromagnetic field, as in the case of acoustic waves by using the hard boundary.

Basic elements in airborne acoustic resonators can be Fabry-Pérot [20], Helmholtz [69], membrane-type resonators [70], etc. By regulating the resonance frequency and oscillation strength, one can always achieve the impedance-matching condition, in principle, by designing the absorber's geometry. Early prototypes of single-band acoustic metamaterial absorbers date back to the microporous panels investigated by Maa [71], who maximized the absorption bandwidth by optimizing the inner diameter and depth of the perforations. Recently, with more well-designed configurations, space-coiling [72–76] and membrane-type structures [77] are proven to support high absorption with thin thickness that is only 1 or even 2 orders magnitude of the relevant wavelength. Donda *et al.* [76] represented an acoustic metasurface targeting for 50-Hz sound, with only 13 mm thickness ($\sim\lambda/523$), as shown in Fig. 6(a). They took advantage of multicoiled channels as an additional degree of freedom to achieve the low-frequency absorption. Ma *et al.* [77] utilized hybrid resonances to create a triple-band membrane-type absorber [see Fig. 6(b)]. They further demonstrated that the unusual large amplitude of the membrane's vibration could be harnessed to effectively generate electrical energy with an efficiency of 23%. To further extend the absorption bandwidth, Jiménez *et al.* [78] constructed stacked Helmholtz resonators (HRs) with different sized cavities [see Fig. 6(c)]. The dimensions of the HRs are optimized by using the algorithm of sequential quadratic programming to realize high absorption from

almost 300 to 1000 Hz. Many other works [79–83] also demonstrated both theoretically and experimentally that broadband behavior could be guaranteed, as long as more resonant states were involved in building the absorber. Interestingly, under the action of natural selection, moths have also evolved microfeathers of different sizes (as multiple resonators) on their wings to broadband absorb the ultrasonic detection signal from their natural enemy, bats [84].

Yang *et al.* [20,85] systematically developed a design scheme for Fabry-Pérot resonances that could analytically predict the required resonance distribution for broadband impedance matching, as shown in Fig. 7(a). The horizontal axis denotes the order of the resonators normalized by the total number, N , while the vertical axis is the logarithm of first-order Fabry-Pérot resonance frequencies, normalized by the lowest $\omega_1 = 2\pi \times 343$ Hz. The gray line represents the ideal resonance distribution for continuum resonances ($N \rightarrow \infty$). But when it comes to the practical sample, only a finite number of resonators can be designed ($N = 16$) [see the red dots in Fig. 7(a) and the corresponding sample in Fig. 7(c)]. Since each Fabry-Pérot resonator can generate an infinite series of resonant states, absorption at high frequencies is usually easy to attain. The resulting performance is plotted in Fig. 7(b), with high absorption starting from 400 Hz. It is reported that the sample thickness (10.86 cm) is slightly larger than the causal minimal thickness (10.36 cm), and thus, $R_c = 1.048$. The same scheme can also be used to customize the absorption spectrum. As an example, by focusing on the absorption within the band of 350–550 and 1200 Hz onwards, the resonance-mode

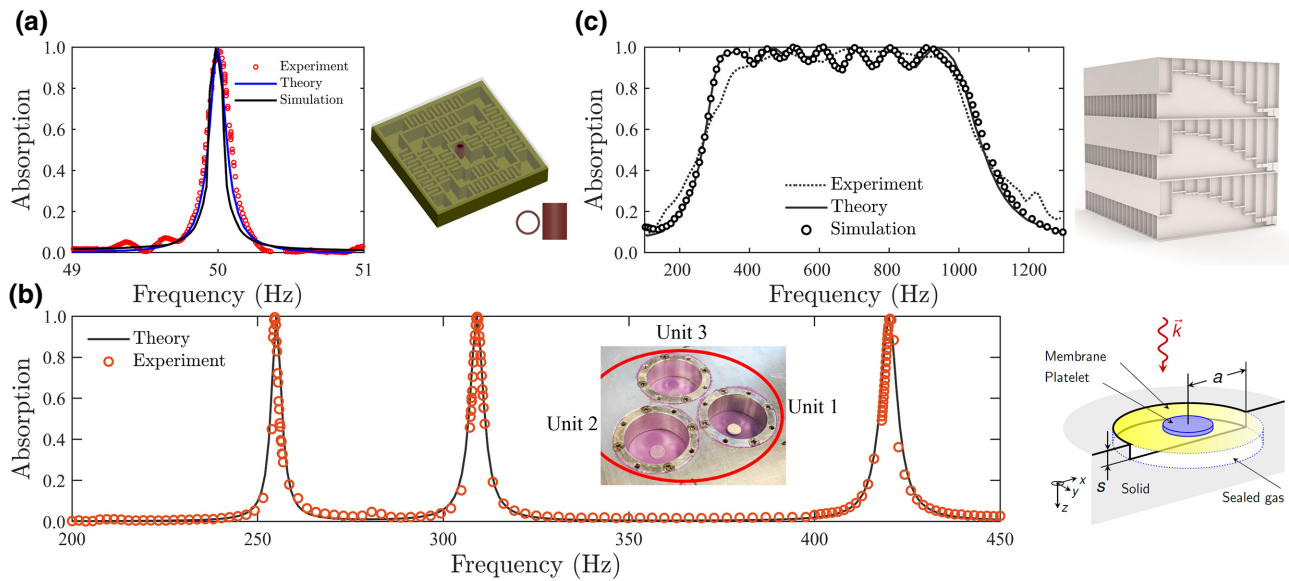


FIG. 6. Performance of acoustic metamaterial absorbers and their structures. (a) Single-band low-frequency absorber with high absorption at 50 Hz. (b) Triple-band absorber with three integrated membrane resonators. Inset shows the fabricated integrated sample, while, on the right side, one unit cell for a single resonator is displayed. (c) Multilayer absorber with wider absorption band, enabled by stacked Helmholtz resonators. Reused with permission from Refs. [76–78].

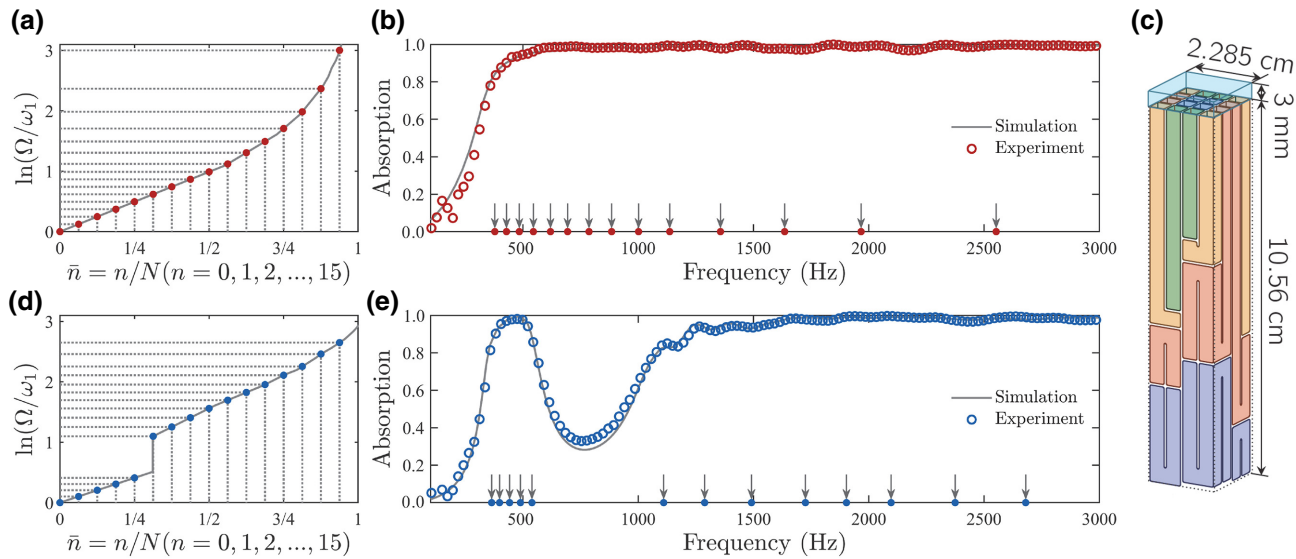


FIG. 7. (a) Scheme for arranging the Fabry-Pérot resonance frequencies (red dots), for broadband impedance matching. (b) Resulting absorption spectrum. Arrows indicate the distribution of resonances on a linear scale (only first-order resonances are plotted here). (c) Schematic of the sample, which is made of 16 air tubes, folded to be a compact structure. On the top, a 3-mm-thick foam is placed to dissipate evanescent waves. (d) Another scheme for customized absorption bands. (e) Resulting customized absorption spectrum. Resonances and absorption are concentrated around 450 Hz and beyond 1100 Hz. Reused with permissions from Ref. [20].

distribution can be updated by using the same algorithm as that for the targeted absorption bands. The latter is shown in Fig. 7(d). The resulting absorption and resonant modes are concentrated around the desired bands [see Fig. 7(e)]. The related sample thickness is 9.33 cm, which is also close to the causal optimality. This customizable strategy is especially useful for the noise source, the intensity distribution of which is mainly concentrated in certain bands. By using metamaterial absorbers, the space resources can be fully utilized to support the desired resonances. It is worth noting that, recently, more metamaterial absorbers use alternative approaches, such as the genetic algorithm [86], particle swarm optimization [87], and graph theory modeling [88], to reach causal optimality using distinct structures.

We note that there is a class of acoustic absorbers [89–93] that operates in applications that require ventilation, i.e., where the rigid backing is replaced by the impedance-matching boundary. This is often the case in acoustic ductworks with noisy fans. By enhancing the oscillation strength of the resonances (stronger than that required by impedance matching), acoustic absorbers can be turned into sound-insulating liners [24,94–99] for a targeted frequency band. In Ref. [100], it was shown that in EM systems different material parameters were required to realize perfect absorption for different back-boundary conditions. For an arbitrary impedance back boundary, whether there are any generalized forms of causality constraint for transmission and/or reflection coefficients remains a topic to be explored. Moreover, if the absorbing layer is anisotropic (see example in Ref. [101]),

the inequality given by Eq. (9) may be adapted to new forms. More theoretical studies are expected to appear in the future for attaining the generalized forms for the causal limit. It should be noted that the design concepts underlying the resonance-based metamaterials have already begun to diffuse to other systems, such as underwater acoustic absorbers [102–104] and elastic wave absorbers [105,106], and thus, these materials have broad application potential.

IV. METASTRUCTURES BEYOND THE CAUSAL LIMIT

The causality principle is perfectly general; it must hold regardless of its target applications. However, the derivation of Eq. (9) involves assumptions other than the causality principle, e.g., the Neumann boundary condition ($\partial_x \phi|_{x=d} = 0$) on the backside of the sample, plus linearity of the sample response, passivity, time invariance, etc. In addition, Eq. (9) is also noted to contain the static material properties μ_{eff} or B_{eff} . By either modifying the auxiliary assumption(s) or using materials with large static μ_{eff} or $1/B_{\text{eff}}$ values, it is entirely possible to, respectively, mitigate or circumvent the stringent constraint imposed by the causal limit. In what follows, we describe some metastructures that use different methods to achieve this goal.

A. Mitigation approach

One can lower factor F in Eq. (9) to provide a greater absorption capacity with the same limited thickness resources or to shrink the sample thickness without

affecting the absorption spectrum. Usually, F is slightly greater than or equal to unity for most of the common EM and airborne acoustic metamaterials with high porosity (defined as the reciprocal of F). To go beyond the original causal limit with $F \geq 1$, we should reduce factor F by introducing materials with large μ_{eff} or small B_{eff} .

In the EM system, this can be done by using magnetic materials [107,108], the static permeability, μ_{eff} , of which is larger than that of the air or vacuum μ_0 . However, since materials with a large static magnetic permeability usually exhibit μ_{eff} that approaches one at microwave frequencies, simply using such materials can only make $R_c \gg 1$. Hence, it is important that the large magnetic permeability values can persist to microwave frequencies. In the absence of such materials, one can use the large relaxational response at microwave frequencies for some magnetic materials to realize a smaller F [109,110], and thus, good low-frequency absorption as well. We note that, although purely metallic structures can generate magnetic responses [111–113], at the static limit ($\omega \rightarrow 0$), the response is still nonmagnetic.

For acoustic systems, a small F requires that the static bulk modulus, B_{eff} , should be smaller than that of the incident medium, B_0 . This is feasible for underwater acoustic metamaterials. It was reported in Ref. [104] that an ultrathin but broadband underwater absorber was tailored to create a small B_{eff} by using a soft composite with high mass density. But whether the same idea can be used to design thinner absorbers in airborne acoustics remains an open question; it is the case that, even though a smaller effective bulk modulus than that of air can be realized in a double-zero medium [114], the desired properties are only valid at a certain frequency but not at the static limit, which is required to realize a small F . In addition, it should be noted that the mitigation approach is still governed by the causal limit, i.e., Eq. (9) still holds but the tight constraint is relaxed.

B. Circumvention approach

Circumvention of the causal constraint means violating some of the auxiliary assumptions used in the derivation of Eq. (9), thereby circumventing the causal constraint. There are several different methods under of this approach.

1. Coherent perfect absorption

Perhaps the best-known examples are coherent perfect absorbers (CPAs) [115]. In these devices, the amplitude, phase, and frequency of the incident wave need to be accurately known prior to launching a coherent antisymmetrical backward wave to interference with it and finally the energy of both forward and backward waves is totally dissipated within an ultrathin lossy layer. The CPA was first discovered in the optical regime [116] and only later in the microwave regime [117,118]. The same concept

was also simultaneously extended to acoustic systems [119–121]. The advantages of the CPA are that its absorption is extremely effective, especially for low-frequency waves, and the thickness is very thin compared with the relevant wavelength. However, the disadvantages are also evident. For example, in principle, it cannot directly work without prior information (amplitude, phase, and frequency). In addition, CPAs essentially rely on a one-dimensional setup (for guiding plane waves), which may not function under random incident angles (e.g., this is often the case in room acoustics).

2. Adding active components

Another way is to introduce active components that can achieve desired material properties with more degrees of freedom [122–124]. In particular, non-Foster elements [125–127] can be incorporated into the original passive EM structures to achieve better low-frequency absorption performance. In Ref. [125], measured results showed that the proposed microwave absorber achieved at least -10 -dB reflection loss from 150 to 900 MHz with only 3 cm thickness. The adopted active non-Foster elements, based on negative-impedance circuits, can create the response not available from the passive systems, which are also used to break the original performance limitation in not only wave absorption but also radiation [128,129], cloaking [130], etc. But, again, we note that the prerequisite information (i.e., amplitude) from the incident wave needs to be known to set the optimal power of the active components [125]. In addition, non-Foster elements should be carefully designed to avoid system instabilities. Although absorbers with active components have much better low-frequency performance, the price to pay is more sophisticated design and possibly higher production cost.

In recent years, with a deeper understanding of non-Hermitian systems [131], perfect absorption at the exceptional points has also attracted more attention due to the anomalous broadened absorption peaks [132,133], as confirmed by recent experiments [134].

3. Temporal switching

The third method is to violate the time-invariance assumption, since the causal limit is derived by Fourier transform to the frequency domain (implying the assumption of time-independent steady states). Hadad *et al.* [135] designed a spatiotemporally modulated device to realize nonreciprocity effects and found that the absorption could be much higher than the emission. Shlivinski and Hadad [136] proposed a temporal-switching transmission line between a source (Z_S) and load (Z_L). In a time-invariant system, the transmission efficiency is limited, especially when $Z_S \gg Z_L$ or $Z_S \ll Z_L$. However, it is found that, if the incident medium's material properties can be switched to another state at the proper time, the efficiency can be

even higher under the high-contrast case. In addition, the same group investigated the particular case in Ref. [137] when the load was replaced by a PEC boundary, and the abrupt switching was improved by gradual switching. The results show that the absorption can be larger than what the causal limit allows. Li and Alù [138] developed a temporal switching absorber as well; its absorption spectrum can be customized according to practical needs.

4. Altering the boundary condition

The fourth method is to alter the boundary condition on the backside of the absorber from Neumann to Dirichlet boundary conditions. The latter represents the PMC boundary condition for the EM case and the soft boundary condition in the acoustic case. Neumann and Dirichlet boundary conditions have a common property: they do not allow the energy transmission of waves (so the system is still one port without energy leaking).

By introducing an acoustic soft-boundary-based absorber (ASBA), Mak *et al.* [139] detailed an alternative route for solving the age-old problem of low-frequency sound absorption. They use the end of an open tube to mimic the acoustic soft boundary, i.e., $p|_{x=d} \cong 0$, and place stacked metallic meshes [Fig. 8(b)] in front of it to dissipate 99.99% of the incident energy at 50 Hz, and the sample thickness is optimized to be only 0.5 cm, which is only 7/10 000 of the wavelength. The absorption is kept at

a high level, beyond 90% from 50 to 500 Hz [the green line in Fig. 8(a)]. It is shown that the same absorption using an absorber backed by the hard boundary will need at least $d_{\min} \cong 80$ cm (an underestimated value, since they only measure down to 50 Hz due to experimental limitations). In this experiment, the impedance at the open-tube end will deviate from the perfect soft one with increasing frequency due to scattering caused by lateral modes [see inset in Fig. 8(a)]. But in the measured range (from 50 to 500 Hz), the transmitted energy is less than 5%, which is negligible, especially when the frequency is low. Therefore, the ASBA has an unparalleled performance in the low-frequency limit, complementing the hard-boundary condition that has advantages at high frequencies. The mechanism of the ASBA is very similar to that of the CPA, relying on a lossy layer with an appropriate thickness to achieve the impedance-matching condition. However, as the soft boundary serves as an antisymmetrical mirror for the incident-wave field, it does not need the information from the incident wave.

In Ref. [139], it was further demonstrated that a soft boundary could lower the impedance-matching frequency of the membrane-type absorber to below its resonance frequency; in contrast to the hard-boundary case [77], the impedance-matching frequency of which should be higher than the resonance frequency. To demonstrate this effect, four membrane resonators backed by a 2-cm-thick cavity with sidewall holes linked to open space are shown

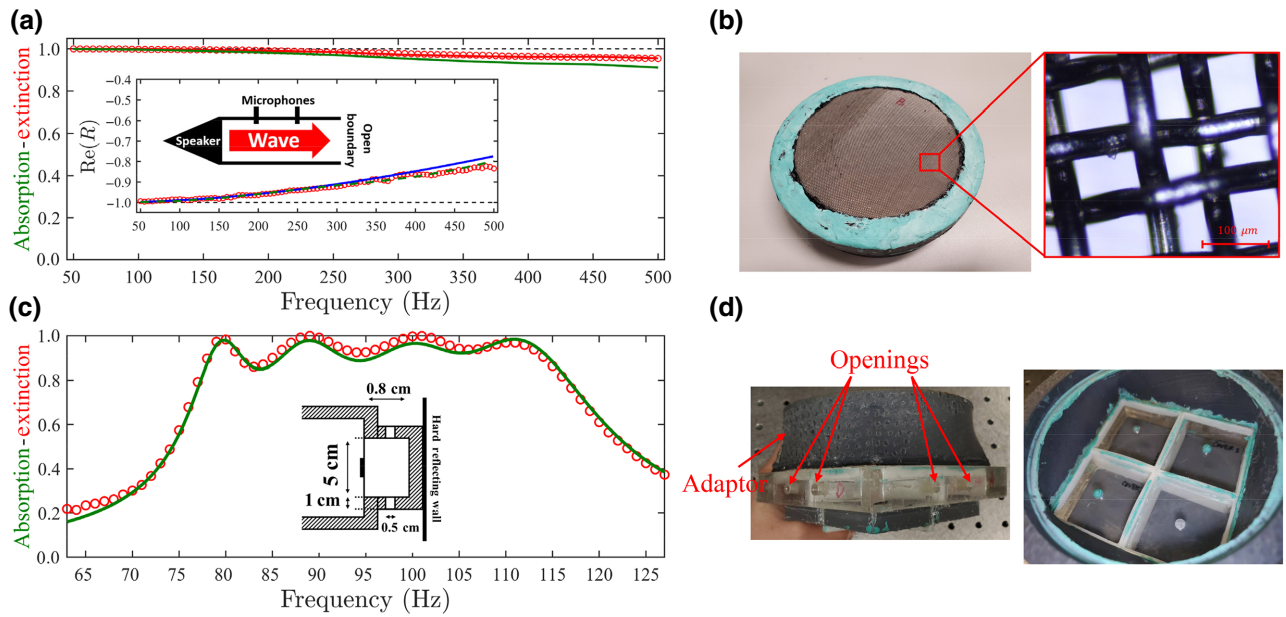


FIG. 8. Metastructure beyond the causal limit by altering the backside boundary condition, from hard to soft boundary. (a) Absorption and extinction spectra. Extinction is defined by $1 - |R|^2$, while the absorption is $A = 1 - |R|^2 - |T|^2$. R and T are reflection and transmission coefficients, respectively. Inset denotes the real part of reflection for an open tube without the sample. (b) Photograph of the metallic mesh used in (a). (c) Absorption-extinction performance of the integrated membrane resonators. (d) Photograph of the fabricated sample with side openings to create a partially soft boundary condition. Left and right photographs denote side and top views, respectively. Reused with permission from Ref. [139].

to display broadband low-frequency absorption (averaged value, 94%) from 80 to 110 Hz [see Fig. 8(c)]. The side-wall holes are crucial for creating the boundary condition that can be characterized as “partially soft boundaries” [see Fig. 8(d)]. The causal limit in this case predicts a minimum thickness of at least 15.1 cm, which is much larger than the sample thickness.

V. CONCLUDING REMARKS

In view of the rapid development of metamaterial absorbers, either under the causal framework or beyond, we conclude that, at the laboratory stage, high absorption performance in most of the targeted frequency bands can now be realized. However, in the transition from scientific discoveries to large-scale applications, factors such as the manufacturing cost need to be considered. As many metamaterials are evolving towards evermore complex geometries [140], mass production cost is becoming an important consideration. We should note that 3D printing technology (mostly used in acoustic metamaterials) is still not a low-cost approach for mass production, and it will face some limitations, especially when multiple materials are involved. Also, when the geometric dimensions are small, accuracy can become a knotty problem. Developing a variety of low-cost manufacturing processes, customized for different types of metamaterials, may alleviate the cost problem of large-scale manufacturing in the future [141,142], e.g., PCB technology may be a promising cheap approach for fabricating EM metamaterials. Meanwhile, the causal limit can also serve as a useful evaluation tool in applications. On one hand, with the assistance of causal limit, engineers can predict whether the given limited space is enough for targeted absorption performance if we use passive absorbers. Or, if the budget and practical situations allow, metastructures beyond the causal limit can be considered. On the other hand, the causality ratio, R_c , can be used to assess the performances of different absorbers, serving as one of the industry standards.

Metamaterial absorbers are envisioned to develop towards a higher degree of performance customization in the future, with diverse structures that can fit into thin and compact volumes, crossing different wave systems. Machine learning and various optimization algorithms [143,144] can assist in building structure-performance networks for the inverse design of the absorbers. The breakthrough in low-cost production technology will inevitably further accelerate the transition from laboratory samples to industrial products.

ACKNOWLEDGMENTS

P.S. acknowledges the support of Grant No. A-HKUST601/18, Research Impact Fund R6015-18, and Grant No. AoE/P-02/12 for this work.

- [1] J.-B. Cheng, H.-G. Shi, M. Cao, T. Wang, H.-B. Zhao, and Y.-Z. Wang, Porous carbon materials for microwave absorption, *Materials Advances* **1**, 2631 (2020).
- [2] J. Allard and N. Atalla, *Propagation of Sound in Porous Media: Modelling Sound Absorbing Materials 2e* (John Wiley & Sons, Hoboken, 2009).
- [3] Y. Ra'Di, C. Simovski, and S. Tretyakov, Thin Perfect Absorbers for Electromagnetic Waves: Theory, Design, and Realizations, *Phys. Rev. Appl.* **3**, 037001 (2015).
- [4] G. Ma and P. Sheng, Acoustic metamaterials: From local resonances to broad horizons, *Sci. Adv.* **2**, e1501595 (2016).
- [5] B. Assouar, B. Liang, Y. Wu, Y. Li, J.-C. Cheng, and Y. Jing, Acoustic metasurfaces, *Nat. Rev. Mater.* **3**, 460 (2018).
- [6] S. A. Cummer, J. Christensen, and A. Alù, Controlling sound with acoustic metamaterials, *Nat. Rev. Mater.* **1**, 16001 (2016).
- [7] Y. Cui, Y. He, Y. Jin, F. Ding, L. Yang, Y. Ye, S. Zhong, Y. Lin, and S. He, Plasmonic and metamaterial structures as electromagnetic absorbers, *Laser Photonics Rev.* **8**, 495 (2014).
- [8] Y. Wu, M. Yang, and P. Sheng, Perspective: Acoustic metamaterials in transition, *J. Appl. Phys.* **123**, 090901 (2018).
- [9] J. Li, X. Wen, and P. Sheng, Acoustic metamaterials, *J. Appl. Phys.* **129**, 171103 (2021).
- [10] J. Mei, G. Ma, M. Yang, Z. Yang, W. Wen, and P. Sheng, Dark acoustic metamaterials as super absorbers for low-frequency sound, *Nat. Commun.* **3**, 756 (2012).
- [11] K. N. Rozanov, Ultimate thickness to bandwidth ratio of radar absorbers, *IEEE Trans. Antennas Propag.* **48**, 1230 (2000).
- [12] O. Acher, J. Bernard, P. Maréchal, A. Bardaine, and F. Levassort, Fundamental constraints on the performance of broadband ultrasonic matching structures and absorbers, *J. Acoust. Soc. Am.* **125**, 1995 (2009).
- [13] M. Yang and P. Sheng, Sound absorption structures: From porous media to acoustic metamaterials, *Annu. Rev. Mater. Res.* **47**, 83 (2017).
- [14] S. Qu, Y. Hou, and P. Sheng, Conceptual-based design of an ultrabroadband microwave metamaterial absorber, *Proc. Natl. Acad. Sci. U. S. A.* **118**, e2110490118 (2021).
- [15] M. Yang, G. Ma, Y. Wu, Z. Yang, and P. Sheng, Homogenization scheme for acoustic metamaterials, *Phys. Rev. B* **89**, 064309 (2014).
- [16] P. Sheng, *Introduction to Wave Scattering, Localization and Mesoscopic Phenomena* (Springer Science & Business Media, New York, 2006), Vol. 88.
- [17] T. Liu, S. Ma, B. Yang, S. Xiao, and L. Zhou, Effective-medium theory for multilayer metamaterials: Role of near-field corrections, *Phys. Rev. B* **102**, 174208 (2020).
- [18] J. D. Jackson, Classical electrodynamics, *Am. Inst. Phys.* **15**, 62 (2009).
- [19] C. A. Dirdal and J. Skaar, Superpositions of Lorentzians as the class of causal functions, *Phys. Rev. A* **88**, 033834 (2013).
- [20] M. Yang, S. Chen, C. Fu, and P. Sheng, Optimal sound-absorbing structures, *Mater. Horiz.* **4**, 673 (2017).
- [21] V. Romero-García, N. Jimenez, G. Theocharis, V. Achilleos, A. Merkel, O. Richoux, V. Tournat,

- J.-P. Groby, and V. Pagneux, Design of acoustic metamaterials made of Helmholtz resonators for perfect absorption by using the complex frequency plane, *C. R. Phys.* **21**, 713 (2020).
- [22] M. Stone and P. Goldbart, *Mathematics for Physics: A Guided Tour for Graduate Students* (Cambridge University Press, Cambridge, UK, 2009).
- [23] S. Qu and P. Sheng, Minimizing Indoor Sound Energy With Tunable Metamaterial Surfaces, *Phys. Rev. Appl.* **14**, 034060 (2020).
- [24] M. Xie, M. Yang, S. Xiao, Y. Xu, and S. Chen, Acoustic Metal, arXiv preprint [arXiv:2010.02813](https://arxiv.org/abs/2010.02813) (2020).
- [25] Y. P. Lee, J. Y. Rhee, Y. J. Yoo, and K. W. Kim, *Metamaterials for Perfect Absorption* (Springer, New York, 2016), p. 113.
- [26] W. Dallenbach and W. Kleinstuber, Reflection and absorption of decimeter-waves by plane dielectric layers, *Hochfreq. u Elektroak* **51**, 152 (1938).
- [27] W. W. Salisbury, Google Patents (1952).
- [28] B. A. Munk, *Frequency Selective Surfaces: Theory and Design* (John Wiley & Sons, Hoboken, 2005).
- [29] A. Serdyukov, I. Semchenko, S. Tretyakov, and A. Silhvol, *Electromagnetics of bi-Anisotropic Materials: Theory and Applications* (Gordon and Breach Science Publishers, Amsterdam, 2001).
- [30] R. L. Fante and M. T. McCormack, Reflection properties of the Salisbury screen, *IEEE Trans. Antennas Propag.* **36**, 1443 (1988).
- [31] N. Landy, S. Sajuyigbe, J. J. Mock, D. R. Smith, and W. J. Padilla, Perfect Metamaterial Absorber, *Phys. Rev. Lett.* **100**, 207402 (2008).
- [32] X. Shen, T. J. Cui, J. Zhao, H. F. Ma, W. X. Jiang, and H. Li, Polarization-independent wide-angle triple-band metamaterial absorber, *Opt. Express* **19**, 9401 (2011).
- [33] F. Ding, Y. Cui, X. Ge, Y. Jin, and S. He, Ultra-broadband microwave metamaterial absorber, *Appl. Phys. Lett.* **100**, 103506 (2012).
- [34] D. Ye, Z. Wang, K. Xu, H. Li, J. Huangfu, Z. Wang, and L. Ran, Ultrawideband Dispersion Control of a Metamaterial Surface for Perfectly-Matched-Layer-Like Absorption, *Phys. Rev. Lett.* **111**, 187402 (2013).
- [35] H.-T. Chen, J. Zhou, J. F. O'Hara, F. Chen, A. K. Azad, and A. J. Taylor, Antireflection Coating Using Metamaterials and Identification of its Mechanism, *Phys. Rev. Lett.* **105**, 073901 (2010).
- [36] X. Liu, T. Starr, A. F. Starr, and W. J. Padilla, Infrared Spatial and Frequency Selective Metamaterial With Near-Unity Absorbance, *Phys. Rev. Lett.* **104**, 207403 (2010).
- [37] X. Liu, T. Tyler, T. Starr, A. F. Starr, N. M. Jokerst, and W. J. Padilla, Taming the Blackbody with Infrared Metamaterials as Selective Thermal Emitters, *Phys. Rev. Lett.* **107**, 045901 (2011).
- [38] B. Wang, T. Koschny, and C. M. Soukoulis, Wide-angle and polarization-independent chiral metamaterial absorber, *Phys. Rev. B* **80**, 033108 (2009).
- [39] X. Shen, Y. Yang, Y. Zang, J. Gu, J. Han, W. Zhang, and T. Jun Cui, Triple-band terahertz metamaterial absorber: Design, experiment, and physical interpretation, *Appl. Phys. Lett.* **101**, 154102 (2012).
- [40] J. W. Park, P. Van Tuong, J. Y. Rhee, K. W. Kim, W. H. Jang, E. H. Choi, L. Y. Chen, and Y. Lee, Multi-band metamaterial absorber based on the arrangement of donut-type resonators, *Opt. Express* **21**, 9691 (2013).
- [41] Y. Cui, J. Xu, K. Hung Fung, Y. Jin, A. Kumar, S. He, and N. X. Fang, A thin film broadband absorber based on multi-sized nanoantennas, *Appl. Phys. Lett.* **99**, 253101 (2011).
- [42] H. Xiong, J.-S. Hong, C.-M. Luo, and L.-L. Zhong, An ultrathin and broadband metamaterial absorber using multi-layer structures, *J. Appl. Phys.* **114**, 064109 (2013).
- [43] J. Gong, F. Yang, Q. Shao, X. He, X. Zhang, S. Liu, L. Tang, and Y. Deng, Microwave absorption performance of methylimidazolium ionic liquids: Towards novel ultra-wideband metamaterial absorbers, *RSC Adv.* **7**, 41980 (2017).
- [44] Z. Shen, X. Huang, H. Yang, T. Xiang, C. Wang, Z. Yu, and J. Wu, An ultra-wideband, polarization insensitive, and wide incident angle absorber based on an irregular metamaterial structure with layers of water, *J. Appl. Phys.* **123**, 225106 (2018).
- [45] F. Yang, J. Gong, E. Yang, Y. Guan, X. He, S. Liu, X. Zhang, and Y. Deng, Ultrabroadband metamaterial absorbers based on ionic liquids, *Appl. Phys. A* **125**, 149 (2019).
- [46] J. Zhao, C. Zhang, Q. Cheng, J. Yang, and T. J. Cui, An optically transparent metasurface for broadband microwave antireflection, *Appl. Phys. Lett.* **112**, 073504 (2018).
- [47] C.-Y. Wang, J.-G. Liang, T. Cai, H.-P. Li, W.-Y. Ji, Q. Zhang, and C.-W. Zhang, High-performance and ultra-broadband metamaterial absorber based on mixed absorption mechanisms, *IEEE Access* **7**, 57259 (2019).
- [48] K.-L. Zhang, J.-Y. Zhang, Z.-L. Hou, S. Bi, and Q.-L. Zhao, Multifunctional broadband microwave absorption of flexible graphene composites, *Carbon* **141**, 608 (2019).
- [49] Y. Huang, W.-L. Song, C. Wang, Y. Xu, W. Wei, M. Chen, L. Tang, and D. Fang, Multi-scale design of electromagnetic composite metamaterials for broadband microwave absorption, *Compos. Sci. Technol.* **162**, 206 (2018).
- [50] Y. Shang, Z. Shen, and S. Xiao, On the design of single-layer circuit analog absorber using double-square-loop array, *IEEE Trans. Antennas Propag.* **61**, 6022 (2013).
- [51] J. Zhao and Y. Cheng, Ultrabroadband microwave metamaterial absorber based on electric SRR loaded with lumped resistors, *J. Electron. Mater.* **45**, 5033 (2016).
- [52] M. Zhang, B. Zhang, X. Liu, S. Sun, and C. Jin, Design of wideband absorber based on dual-resistor-loaded metallic strips, *Int. J. Antennas Propag.* **2020**, 1238656 (2020).
- [53] D. Ye, Z. Wang, Z. Wang, K. Xu, B. Zhang, J. Huangfu, C. Li, and L. Ran, Towards experimental perfectly-matched layers with ultra-thin metamaterial surfaces, *IEEE Trans. Antennas Propag.* **60**, 5164 (2012).
- [54] X. Li, M. Pu, X. Ma, Y. Guo, P. Gao, and X. Luo, Dispersion engineering in metamaterials and metasurfaces, *J. Phys. D: Appl. Phys.* **51**, 054002 (2018).
- [55] Y. Shen, Z. Pei, Y. Pang, J. Wang, A. Zhang, and S. Qu, An extremely wideband and lightweight metamaterial absorber, *J. Appl. Phys.* **117**, 224503 (2015).
- [56] W.-L. Song, Z. Zhou, L.-C. Wang, X.-D. Cheng, M. Chen, R. He, H. Chen, Y. Yang, and D. Fang, Constructing repairable meta-structures of ultra-broad-band electromagnetic absorption from three-dimensional printed

- patterned shells, *ACS Appl. Mater. Interfaces* **9**, 43179 (2017).
- [57] W. Xu and S. Sonkusale, Microwave diode switchable metamaterial reflector/absorber, *Appl. Phys. Lett.* **103**, 031902 (2013).
- [58] Q. Zhou, X. Yin, F. Ye, R. Mo, Z. Tang, X. Fan, L. Cheng, and L. Zhang, Optically transparent and flexible broadband microwave metamaterial absorber with sandwich structure, *Appl. Phys. A* **125**, 131 (2019).
- [59] H. Tao, N. I. Landy, C. M. Bingham, X. Zhang, R. D. Averitt, and W. J. Padilla, A metamaterial absorber for the terahertz regime: Design, fabrication and characterization, *Opt. Express* **16**, 7181 (2008).
- [60] Q.-Y. Wen, H.-W. Zhang, Y.-S. Xie, Q.-H. Yang, and Y.-L. Liu, Dual band terahertz metamaterial absorber: Design, fabrication, and characterization, *Appl. Phys. Lett.* **95**, 241111 (2009).
- [61] Z. Shen, S. Li, Y. Xu, W. Yin, L. Zhang, and X. Chen, Three-Dimensional Printed Ultrabroadband Terahertz Metamaterial Absorbers, *Phys. Rev. Appl.* **16**, 014066 (2021).
- [62] G. Dayal and S. A. Ramakrishna, Design of highly absorbing metamaterials for infrared frequencies, *Opt. Express* **20**, 17503 (2012).
- [63] C. T. Riley, J. S. Smalley, J. R. Brodie, Y. Fainman, D. J. Siblly, and Z. Liu, Near-perfect broadband absorption from hyperbolic metamaterial nanoparticles, *Proc. Natl. Acad. Sci.* **114**, 1264 (2017).
- [64] K. Aydin, V. E. Ferry, R. M. Briggs, and H. A. Atwater, Broadband polarization-independent resonant light absorption using ultrathin plasmonic super absorbers, *Nat. Commun.* **2**, 571 (2011).
- [65] Y. Huang, L. Liu, M. Pu, X. Li, X. Ma, and X. Luo, A refractory metamaterial absorber for ultra-broadband, omnidirectional and polarization-independent absorption in the UV-NIR spectrum, *Nanoscale* **10**, 8298 (2018).
- [66] H. Fan, J. Li, Y. Lai, and J. Luo, Optical Brewster Metasurfaces Exhibiting Ultrabroadband Reflectionless Absorption and Extreme Angular Asymmetry, *Phys. Rev. Appl.* **16**, 044064 (2021).
- [67] A. P. Raman, M. Abou Anoma, L. Zhu, E. Rephaeli, and S. Fan, Passive radiative cooling below ambient air temperature under direct sunlight, *Nature* **515**, 540 (2014).
- [68] Z. Yu, A. Raman, and S. Fan, Fundamental limit of nanophotonic light trapping in solar cells, *Proc. Natl. Acad. Sci.* **107**, 17491 (2010).
- [69] N. Fang, D. Xi, J. Xu, M. Ambati, W. Srituravanich, C. Sun, and X. Zhang, Ultrasonic metamaterials with negative modulus, *Nat. Mater.* **5**, 452 (2006).
- [70] Z. Yang, J. Mei, M. Yang, N. Chan, and P. Sheng, Membrane-Type Acoustic Metamaterial With Negative Dynamic Mass, *Phys. Rev. Lett.* **101**, 204301 (2008).
- [71] D.-Y. Maa, Potential of microperforated panel absorber, *J. Acoust. Soc. Am.* **104**, 2861 (1998).
- [72] Y. Li and B. M. Assouar, Acoustic metasurface-based perfect absorber with deep subwavelength thickness, *Appl. Phys. Lett.* **108**, 063502 (2016).
- [73] X. Cai, Q. Guo, G. Hu, and J. Yang, Ultrathin low-frequency sound absorbing panels based on coplanar spiral tubes or coplanar Helmholtz resonators, *Appl. Phys. Lett.* **105**, 121901 (2014).
- [74] H. Long, Y. Cheng, J. Tao, and X. Liu, Perfect absorption of low-frequency sound waves by critically coupled subwavelength resonant system, *Appl. Phys. Lett.* **110**, 023502 (2017).
- [75] N. Jiménez, W. Huang, V. Romero-García, V. Pagneux, and J.-P. Groby, Ultra-thin metamaterial for perfect and quasi-omnidirectional sound absorption, *Appl. Phys. Lett.* **109**, 121902 (2016).
- [76] K. Donda, Y. Zhu, S.-W. Fan, L. Cao, Y. Li, and B. Assouar, Extreme low-frequency ultrathin acoustic absorbing metasurface, *Appl. Phys. Lett.* **115**, 173506 (2019).
- [77] G. Ma, M. Yang, S. Xiao, Z. Yang, and P. Sheng, Acoustic metasurface with hybrid resonances, *Nat. Mater.* **13**, 873 (2014).
- [78] N. Jiménez, V. Romero-García, V. Pagneux, and J.-P. Groby, Rainbow-trapping absorbers: Broadband, perfect and asymmetric sound absorption by subwavelength panels for transmission problems, *Sci. Rep.* **7**, 13595 (2017).
- [79] X. Jiang, B. Liang, R.-Q. Li, X.-Y. Zou, L.-L. Yin, and J.-C. Cheng, Ultra-broadband absorption by acoustic metamaterials, *Appl. Phys. Lett.* **105**, 243505 (2014).
- [80] J. Li, W. Wang, Y. Xie, B.-I. Popa, and S. A. Cummer, A sound absorbing metasurface with coupled resonators, *Appl. Phys. Lett.* **109**, 091908 (2016).
- [81] V. Romero-García, G. Theocharis, O. Richoux, and V. Pagneux, Use of complex frequency plane to design broadband and sub-wavelength absorbers, *J. Acoust. Soc. Am.* **139**, 3395 (2016).
- [82] H. Long, C. Shao, C. Liu, Y. Cheng, and X. Liu, Broadband near-perfect absorption of low-frequency sound by subwavelength metasurface, *Appl. Phys. Lett.* **115**, 103503 (2019).
- [83] Y. Zhu, A. Merkel, K. Donda, S. Fan, L. Cao, and B. Assouar, Nonlocal acoustic metasurface for ultrabroadband sound absorption, *Phys. Rev. B* **103**, 064102 (2021).
- [84] T. R. Neil, Z. Shen, D. Robert, B. W. Drinkwater, and M. W. Holdried, Moth wings are acoustic metamaterials, *Proc. Natl. Acad. Sci.* **117**, 31134 (2020).
- [85] M. Yang and P. Sheng, An integration strategy for acoustic metamaterials to achieve absorption by design, *Appl. Sci.* **8**, 1247 (2018).
- [86] Z. Zhou, S. Huang, D. Li, J. Zhu, and Y. Li, Broadband impedance modulation via non-local acoustic metamaterials, *Nat. Sci. Rev., nwab171* (2021).
- [87] T. Bravo and C. Maury, Causally-guided acoustic optimization of rigidly-backed micro-perforated partitions: Case studies and experiments, *J. Sound Vib.* **523**, 116735 (2022).
- [88] I. Davis, A. McKay, and G. J. Bennett, A graph-theory approach to optimisation of an acoustic absorber targeting a specific noise spectrum that approaches the causal optimum minimum depth, *J. Sound Vib.* **505**, 116135 (2021).
- [89] M. Yang, C. Meng, C. Fu, Y. Li, Z. Yang, and P. Sheng, Subwavelength total acoustic absorption with degenerate resonators, *Appl. Phys. Lett.* **107**, 104104 (2015).
- [90] V. Romero-García, N. Jiménez, J.-P. Groby, A. Merkel, V. Tournat, G. Theocharis, O. Richoux, and V. Pagneux, Perfect Absorption in Mirror-Symmetric Acoustic Metascreens, *Phys. Rev. Appl.* **14**, 054055 (2020).

- [91] X. Wu, K. Y. Au-Yeung, X. Li, R. C. Roberts, J. Tian, C. Hu, Y. Huang, S. Wang, Z. Yang, and W. Wen, High-efficiency ventilated metamaterial absorber at low frequency, *Appl. Phys. Lett.* **112**, 103505 (2018).
- [92] T. Lee, T. Nomura, E. M. Dede, and H. Iizuka, Ultrasparse Acoustic Absorbers Enabling Fluid Flow and Visible-Light Controls, *Phys. Rev. Appl.* **11**, 024022 (2019).
- [93] N. Gao, S. Qu, J. Li, J. Wang, and W. Chen, Harnessing post-buckling deformation to tune sound absorption in soft Helmholtz absorbers, *Int. J. Mech. Sci.* **208**, 106695 (2021).
- [94] Y. Cheng, C. Zhou, B. Yuan, D. Wu, Q. Wei, and X. Liu, Ultra-sparse metasurface for high reflection of low-frequency sound based on artificial Mie resonances, *Nat. Mater.* **14**, 1013 (2015).
- [95] C. Liu, J. Shi, W. Zhao, X. Zhou, C. Ma, R. Peng, M. Wang, Z. H. Hang, X. Liu, J. Christensen, and N. X. Fang, Three-Dimensional Soundproof Acoustic Metacage, *Phys. Rev. Lett.* **127**, 084301 (2021).
- [96] H.-L. Zhang, Y.-F. Zhu, B. Liang, J. Yang, J. Yang, and J.-C. Cheng, Omnidirectional ventilated acoustic barrier, *Appl. Phys. Lett.* **111**, 203502 (2017).
- [97] X. Su and D. Banerjee, Extraordinary Sound Isolation Using an Ultrasparse Array of Degenerate Anisotropic Scatterers, *Phys. Rev. Appl.* **13**, 064047 (2020).
- [98] M. Sun, X. Fang, D. Mao, X. Wang, and Y. Li, Broadband Acoustic Ventilation Barriers, *Phys. Rev. Appl.* **13**, 044028 (2020).
- [99] S.-W. Fan, S.-D. Zhao, A.-L. Chen, Y.-F. Wang, B. Assouar, and Y.-S. Wang, Tunable Broadband Reflective Acoustic Metasurface, *Phys. Rev. Appl.* **11**, 044038 (2019).
- [100] J. Luo, S. Li, B. Hou, and Y. Lai, Unified theory for perfect absorption in ultrathin absorptive films with constant tangential electric or magnetic fields, *Phys. Rev. B* **90**, 165128 (2014).
- [101] J. Luo, H. Chu, R. Peng, M. Wang, J. Li, and Y. Lai, Ultra-broadband reflectionless Brewster absorber protected by reciprocity, *Light: Sci. Appl.* **10**, 89 (2021).
- [102] Y. Zhang, K. A. Chen, X. Hao, and Y. Cheng, A review of underwater acoustic metamaterials, *Chin. Sci. Bull.* **65**, 1396 (2020).
- [103] M. Duan, C. Yu, F. Xin, and T. J. Lu, Tunable underwater acoustic metamaterials via quasi-Helmholtz resonance: From low-frequency to ultra-broadband, *Appl. Phys. Lett.* **118**, 071904 (2021).
- [104] S. Qu, N. Gao, A. Tinel, B. Morvan, V. Romero-García, J.-P. Groby, and P. Sheng, Underwater metamaterial absorber with impedance-matched composite, arXiv preprint [arXiv:2111.02075](https://arxiv.org/abs/2111.02075) (2021).
- [105] L. Cao, Z. Yang, Y. Xu, S.-W. Fan, Y. Zhu, Z. Chen, Y. Li, and B. Assouar, Flexural wave absorption by lossy gradient elastic metasurface, *J. Mech. Phys. Solids* **143**, 104052 (2020).
- [106] X. Li, Y. Chen, R. Zhu, and G. Huang, An active meta-layer for optimal flexural wave absorption and cloaking, *Mech. Syst. Signal Process.* **149**, 107324 (2021).
- [107] A. Raveendran, M. T. Sebastian, and S. Raman, Applications of microwave materials: A review, *J. Electron. Mater.* **48**, 2601 (2019).
- [108] J. Ning, S. Dong, X. Luo, K. Chen, J. Zhao, T. Jiang, and Y. Feng, Ultra-broadband microwave absorption by ultra-thin metamaterial with stepped structure induced multi-resonances, *Results Phys.* **18**, 103320 (2020).
- [109] B.-Y. Zong, Z.-W. Pong, Y.-P. Wu, P. Ho, J.-J. Qiu, L.-B. Kong, L. Wang, and G.-C. Han, Electrodeposition of granular FeCoNi films with large permeability for microwave applications, *J. Mater. Chem.* **21**, 16042 (2011).
- [110] Y. Zhao, L. Liu, K. Jiang, M. Fan, C. Jin, J. Han, W. Wu, and G. Tong, Distinctly enhanced permeability and excellent microwave absorption of expanded graphite/Fe₃O₄ nanoring composites, *RSC Adv.* **7**, 11561 (2017).
- [111] D. Schurig, J. J. Mock, B. J. Justice, S. A. Cummer, J. B. Pendry, A. F. Starr, and D. R. Smith, Metamaterial electromagnetic cloak at microwave frequencies, *Science* **314**, 977 (2006).
- [112] T.-J. Yen, W. Padilla, N. Fang, D. Vier, D. Smith, J. Pendry, D. Basov, and X. Zhang, Terahertz magnetic response from artificial materials, *Science* **303**, 1494 (2004).
- [113] J. B. Pendry, A. J. Holden, D. J. Robbins, and W. Stewart, Magnetism from conductors and enhanced nonlinear phenomena, *IEEE Trans. Microw. Theory Tech.* **47**, 2075 (1999).
- [114] M. Dubois, C. Shi, X. Zhu, Y. Wang, and X. Zhang, Observation of acoustic Dirac-like cone and double zero refractive index, *Nat. Commun.* **8**, 14871 (2017).
- [115] D. G. Baranov, A. Krasnok, T. Shegai, A. Alù, and Y. Chong, Coherent perfect absorbers: Linear control of light with light, *Nat. Rev. Mater.* **2**, 17064 (2017).
- [116] Y. Chong, L. Ge, H. Cao, and A. D. Stone, Coherent Perfect Absorbers: Time-Reversed Lasers, *Phys. Rev. Lett.* **105**, 053901 (2010).
- [117] Y. Sun, W. Tan, H.-Q. Li, J. Li, and H. Chen, Experimental Demonstration of a Coherent Perfect Absorber With PT Phase Transition, *Phys. Rev. Lett.* **112**, 143903 (2014).
- [118] S. Li, J. Luo, S. Anwar, S. Li, W. Lu, Z. H. Hang, Y. Lai, B. Hou, M. Shen, and C. Wang, Broadband perfect absorption of ultrathin conductive films with coherent illumination: Superabsorption of microwave radiation, *Phys. Rev. B* **91**, 220301 (2015).
- [119] J. Song, P. Bai, Z. Hang, and Y. Lai, Acoustic coherent perfect absorbers, *New J. Phys.* **16**, 033026 (2014).
- [120] Y. Duan, J. Luo, G. Wang, Z. H. Hang, B. Hou, J. Li, P. Sheng, and Y. Lai, Theoretical requirements for broadband perfect absorption of acoustic waves by ultra-thin elastic meta-films, *Sci. Rep.* **5**, 12139 (2015).
- [121] P. Wei, C. Croënne, S. Tak Chu, and J. Li, Symmetrical and anti-symmetrical coherent perfect absorption for acoustic waves, *Appl. Phys. Lett.* **104**, 121902 (2014).
- [122] C. Cho, X. Wen, N. Park, and J. Li, Digitally virtualized atoms for acoustic metamaterials, *Nat. Commun.* **11**, 251 (2020).
- [123] B.-I. Popa, L. Zigoneanu, and S. A. Cummer, Tunable active acoustic metamaterials, *Phys. Rev. B* **88**, 024303 (2013).
- [124] F. Zangeneh-Nejad and R. Fleury, Active times for acoustic metamaterials, *Rev. Phys.* **4**, 100031 (2019).

- [125] J. Mou and Z. Shen, Design and experimental demonstration of non-foster active absorber, *IEEE Trans. Antennas Propag.* **65**, 696 (2016).
- [126] Z. Cheng, S. Xiao, Y. Zhixin, Z. Jiang, and Y. Li, On the design of ultra-low profile broadband absorber based on non-Foster circuit, *IEEE Antennas Wirel. Propag.* **21**, 600 (2021).
- [127] Y. Fan, H. C. Zhang, J. Y. Yin, L. Xu, D. S. Nagarkoti, Y. Hao, and T. J. Cui, An active wideband and wide-angle electromagnetic absorber at microwave frequencies, *IEEE Antennas Wirel. Propag. Lett.* **15**, 1913 (2016).
- [128] C. Rasmussen and A. Alù, Non-Foster acoustic radiation from an active piezoelectric transducer, *Proc. Natl. Acad. Sci.* **118**, e2024984118 (2021).
- [129] M. M. Jacob, *Non-Foster Circuits for High Performance Antennas: Advantages and Practical Limitations* (University of California, San Diego, 2016).
- [130] P.-Y. Chen, C. Argyropoulos, and A. Alù, Broadening the Cloaking Bandwidth With Non-Foster Metasurfaces, *Phys. Rev. Lett.* **111**, 233001 (2013).
- [131] Z. Gu, H. Gao, P.-C. Cao, T. Liu, X.-F. Zhu, and J. Zhu, Controlling Sound in Non-Hermitian Acoustic Systems, *Phys. Rev. Appl.* **16**, 057001 (2021).
- [132] V. Achilleos, G. Theocharis, O. Richoux, and V. Pagneux, Non-Hermitian acoustic metamaterials: Role of exceptional points in sound absorption, *Phys. Rev. B* **95**, 144303 (2017).
- [133] W. R. Sweeney, C. W. Hsu, S. Rotter, and A. D. Stone, Perfectly Absorbing Exceptional Points and Chiral Absorbers, *Phys. Rev. Lett.* **122**, 093901 (2019).
- [134] C. Wang, W. R. Sweeney, A. D. Stone, and L. Yang, Coherent perfect absorption at an exceptional point, *Science* **373**, 1261 (2021).
- [135] Y. Hadad, J. C. Soric, and A. Alù, Breaking temporal symmetries for emission and absorption, *Proc. Natl. Acad. Sci.* **113**, 3471 (2016).
- [136] A. Shlivinski and Y. Hadad, Beyond the Bode-Fano Bound: Wideband Impedance Matching for Short Pulses Using Temporal Switching of Transmission-Line Parameters, *Phys. Rev. Lett.* **121**, 204301 (2018).
- [137] C. Firestein, A. Shlivinski, and Y. Hadad, Absorption and Scattering by a Temporally Switched Lossy Layer: Going Beyond the Rozanov Bound, *Phys. Rev. Appl.* **17**, 014017 (2022).
- [138] H. Li and A. Alù, Temporal switching to extend the bandwidth of thin absorbers, *Optica* **8**, 24 (2021).
- [139] H. Y. Mak, X. Zhang, Z. Dong, S. Miura, T. Iwata, and P. Sheng, Going Beyond the Causal Limit in Acoustic Absorption, *Phys. Rev. Appl.* **16**, 044062 (2021).
- [140] M. Kadic, G. W. Milton, M. van Hecke, and M. Wegener, 3D metamaterials, *Nat. Rev. Phys.* **1**, 198 (2019).
- [141] M. Askari, D. A. Hutchins, P. J. Thomas, L. Astolfi, R. L. Watson, M. Abdi, M. Ricci, S. Laureti, L. Nie, S. Freear, *et al.*, Additive manufacturing of metamaterials: A review, *Addit. Manuf.* **36**, 101562 (2020).
- [142] J. Fan, L. Zhang, S. Wei, Z. Zhang, S.-K. Choi, B. Song, and Y. Shi, A review of additive manufacturing of metamaterials and developing trends, *Mater. Today* **50**, 303 (2021).
- [143] Z.-H. Michalopoulou, P. Gerstoft, B. Kostek, and M. A. Roch, Introduction to the special issue on machine learning in acoustics, *J. Acoust. Soc. Am.* **150**, 3204 (2021).
- [144] Y. Jin, L. He, Z. Wen, B. Mortazavi, H. Guo, D. Torrent, B. Djafari-Rouhani, T. Rabczuk, X. Zhuang, and Y. Li, Intelligent on-demand design of phononic metamaterials, *Nanophotonics* **11**, 439 (2022).